



Synergy effect of boron and cobalt in B₂O₃-SBA-15-(Co)Mo catalyst for efficient hydrodesulfurization of liquid fuels

Saheed A. Ganiyu¹

Received: 14 August 2020 / Accepted: 19 April 2021

© The Author(s), under exclusive licence to Springer Nature B.V. 2021

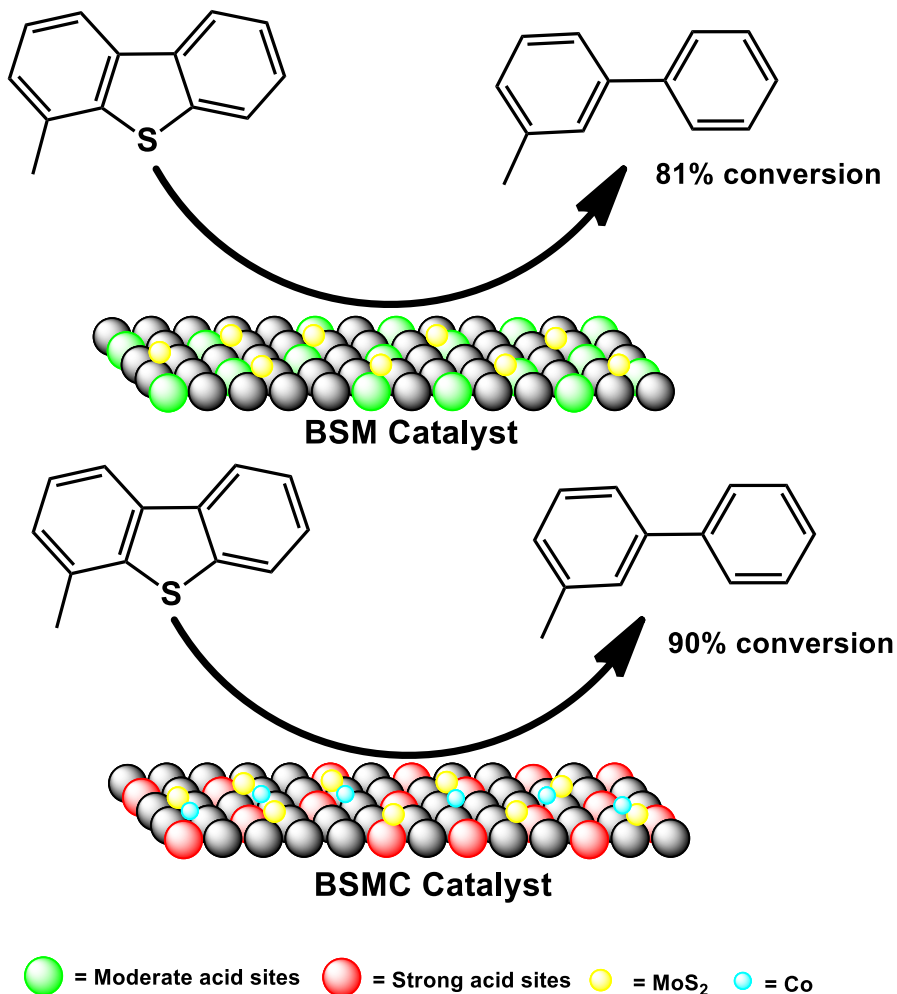
Abstract

The contributory effect of surface acidity is significant to desulfurize heavy recalcitrant organosulfur compounds effectively. This research explores the synergistic effect of boron and cobalt in CoMoS supported on B₂O₃-SBA-15 for ultradeep hydrodesulfurization (HDS) of DBT and MDBT in the model and diesel fuel, respectively. The catalysts prepared consisting of SBA-15-(Co)Mo, representing (SM and SMC) and B₂O₃-SBA-15-(Co)Mo for BSM and BSMC, were fully characterized to gain insight into the structural activity concerning the nature of the fuel and the organosulfur compound employed. The incorporation of boron into the mesoporous framework of SBA-15 improves the surface characteristics, viz. surface acidity, support metal interaction and textural properties, necessary for efficient catalytic HDS reaction. The catalysts BSM and BSMC outperformed their analogous catalysts SM and SMC. The catalytic efficiency of BSMC is outstanding and capable of desulfurizing diesel fuel (1000 ppmw-S) containing a more complex matrix with a 90% conversion of methyl dibenzothiophene (MDBT). BSMC possessed favorable and lower activation energy (E_a) of 77.11 kJ mol⁻¹ than other catalysts and can be used as a commercial catalyst for ultradeep desulfurization of real fuel.

✉ Saheed A. Ganiyu
gsadewale@kfupm.edu.sa

¹ Department of Chemistry, King Fahd University of Petroleum and Minerals, Dhahran 31261, Saudi Arabia

Graphic abstract



Keywords Boron-SBA-15 · CoMo catalysts · Hydrodesulfurization · Diesel · Dibenzothiophene · Methyl dibenzothiophene

Introduction

The stringent environmental regulations imposed on transportation fuels by US and EU agencies to lower the amount of sulfur to as low as 10 ppm and the demand for sulfur-free fuel for automobile catalytic converter have been the motivation for the continued search for robust, highly dispersed and stable hydrodesulfurization (HDS) catalysts [1–6].

HDS of heavier organosulfur compounds such as DBT and alkylated derivatives requires highly porous support with sufficient dispersion of active nanospecies (Ni(Co)Mo(W)) for efficient diffusion and catalytic conversion of the reactants within a short time [7]. The HDS catalytic efficiency of the catalysts is attributed to the physicochemical properties of the support and the catalysts (Ni(Co)Mo(W)). The properties include but not limited to the nature of the support, acidity, surface area, pore size and volume of both support and catalyst, dispersion, reducibility and stability of the catalyst active species [8, 9]. The role and influence of support in catalyst development for heterogeneous reactions are crucial. The properties of supports are mostly proportional to the catalytic efficiency. Alumina-supported catalysts are characterized by high surface acid sites and amorphous pore structures, with thermal and mechanical stability [10]. Lately, research in HDS catalysts' development has been directed towards replacing gamma-Al₂O₃-Ni(Co)Mo(W) due to its strong metal-support interaction (SMSI) from the Type-1 active phase that consequently resulted in low catalytic activity and quick deactivation [11–14].

Furthermore, the alumina metal oxide support generally suffers from the low surface area, which led to low catalytic activity [15]. Molecular sieves (mesoporous) are a group of silica supports used as an alternative to alumina due to their large surface area, ordered porous structure, thermal stability and ease of preparation with tunable physicochemical properties [16–19]. These supports have boosted the high dispersion of active species and better catalytic performance compared to alumina. However, the main challenge with mesoporous silica is the weak metal-support interaction and low support acidity, which resulted from the amorphous nature of the silica wall [20]. The interaction of active metals with silica-based supports is usually enhanced by integrating heteroatoms, such as Ti, Zr, Nb and Al, and is becoming a more pragmatic approach to improve the catalytic activity [21–23]. The addition of additives, such as fluorine, phosphates and chelating agents, has been reported to improve the HDS catalytic activity by improving the dispersion of active species through moderate metal-support interaction [24–28]. The moderate metal-support interaction favors the formation of polyanions (polymolybdates or polytungstates), which are readily sulfided to form molybdenum sulfide (MoS₂) or tungstic sulfide (WS₂) crystallites. The heteroatoms' incorporation to mesoporous silica enhanced the support acidity (both Lewis and Brønsted). It has been reported that the addition of Zr and Ti to the framework of SBA-15 support in the SBA-15-NiMo catalyst increased the available active sites of the catalyst by increasing the acid sites (Lewis) in the modified supported catalyst [29, 30].

Boron, a heteroatom belonging to the metalloid group of elements and with chemical properties closer to aluminum, has been used for numerous catalytic applications [31–34], including HDS [35–37]. Mostly, boron is employed as a stabilizer for sulfided Ni(Co)Mo(W)-supported alumina. Usman et al. optimized the weight percent loading of boron on MoS₂/B/Al₂O₃ and Co-MoS₂/B/Al₂O₃ for thiophene HDS and discovered that 0.6 wt.% of boron gives the best HDS experience [36]. The findings of Rashidi et al. described the combined effect of phosphorus and boron on nano-alumina support that was impregnated with Co and Mo. They discovered that the combined heteroatoms resulted in the catalysts' suitable physicochemical properties that led to high HDS activity [37].

Inspired by boron's role on the catalytic property of Al_2O_3 -CoMo catalysts, boron was incorporated into the mesoporous silica framework and studied the support effect on the HDS reaction of dibenzothiophene (DBT) and methyl dibenzothiophene (MDBT). After a thorough literature search and to the best of the author's knowledge, no known study has been reported on the role of boron on the structural properties and HDS activity of mesoporous silica (SBA-15)-supported CoMo catalysts. The catalyst performance was compared with the analogous CoMo/Al-SBA-15 catalyst. The structural reactivity of the catalysts was investigated by N_2 -physisorption, DRS-UV-Vis spectroscopy, NH_3 -TPD, H_2 -TPR, XRD, Raman, Pyridine FTIR, FESEM and XPS.

Methodology

Synthesis of boron-modified SBA-15-Mo with and without Co (boron-SBA-15-Mo and/or boron-SBA-15-Mo/Co)

The boron-modified mesoporous SBA-15-Mo catalyst was synthesized by incorporating boron and molybdenum into a synthesis mixture containing silica described by Zhao et al. [38]. Firstly, an equivalent of 13 wt.% Mo from ammonium molybdate (VI) tetrahydrate precursor solution was added to a continuously stirred sol solution containing 60 g of 2 M HCl, 4.16 g of TEOS, 2 g of P123 and 15 g of deionized water. The solution mixture was further stirred for 12 h before hydrothermal treatment at 90 °C for 1 day. The resultant white powder, after centrifugation and drying, was calcined to form SBA-15-Mo. Boron and/or cobalt was introduced into the SBA-15-Mo catalyst by adding an equivalent of $\text{Si/B} = 10$ of boron from boric acid precursor solution and/or 3 wt% equivalence of Co from CoCl_2 solution, respectively, to the solution of SBA-15-Mo before the hydrothermal treatment. The details of the catalysts' description can be found in Table SI-1. The as-prepared catalysts described in Table 1 were pelletized to within 300–500 microns before activation and HDS evaluation.

Characterization of catalysts

The catalysts surface area (SA), pore size and pore volume (PSPV) measurements were conducted on a Micromeritics ASAP 2020. The analysis involves degassing of catalysts at 250 °C for 3 h; afterwards, the N_2 isotherms (adsorption-desorption) were measured at 77 K. The XRD pattern of the catalysts was measured on a Rigaku Ultima IV X-ray diffractometer in the range $2\theta = 10^\circ$ – 70° and with a scanning speed of $10^\circ/\text{min}$. The mesoporous diffraction peak of SBA-15 was used to determine pore wall thickness of catalysts after incorporation metals, using SAXS. The functional groups in the catalysts were elucidated through the HORIBA, iHR320 Raman spectroscope with a CCD detector and a laser wavelength of 532 nm. UV-Vis diffuse reflectance spectroscopy (DRS) studies were done on diffuse reflectance-attached Hitachi U-4100 UV-Vis spectrophotometer. The elemental analysis was determined

Table 1 Textural properties of HDS catalysts and pyridine. (Error = ± 2.0%)

Sample	BET surface area (m ² /g)	Micropore area (m ² /g)	External surface area (m ² /g)	Total pore volume (cm ³ /g)	Pore diameter (adsorption) (nm)	d ₁₀₀ (nm)	Pore wall thickness (nm)	L (μmol/g)	B (μmol/g)	Acid density (μmol/m ²)
<i>SBA-15</i>	639	48	591	1.07	6.60	9.77	4.68	—	—	—
<i>SM</i>	536	39	497	0.97	7.21	8.44	2.54	263	99	0.68
<i>SMC</i>	544	82	462	0.8	6.58	8.23	2.92	169	70	0.44
<i>BSM</i>	580	61	519	0.93	6.86	10.21	4.93	359	142	0.86
<i>BSMC</i>	492	45	447	0.86	7.04	9.63	4.08	272	83	0.72

Pore wall thickness = a_0 – pore diameter, $a_0 = 2d_{100}/\sqrt{3}$

by ICP-OES PlasmaQuant Analytic Jena, after the sample (about 100 mg) was well digested in an acidic mixture containing concentrated HNO_3 and HCl (9:1, respectively). The analysis was done in the region of 200–800 nm at ambient temperature. The H_2 -TPR and NH_3 -TPD analyses of the catalysts' oxides were measured using an AutoChem II-2920 Micromeritics Chemisorption analyzer with hydrogen and ammonia, a probe molecule, respectively. The analyses were performed by degassing 100 mg of the catalysts at 500 °C for one hour and cooling to room temperature, both under the 99.99% pure helium flow. Later, 10% H_2 in helium (for H_2 -TPR) was flowed through the catalysts at a 20 ml/min rate, and the amount of H_2 consumed at the reducible temperature (elevated to 1000 °C at a 10 °C/min rate) was recorded. Similarly, the NH_3 -TPD was carried out by flowing 10 wt.% NH_3 to the degassed catalysts at 100 °C for 0.5 h, and the surplus NH_3 was ejected by purging 99.99% pure helium for 1 h. The catalysts were subsequently heated to 800 °C at 10 °C/min, and the desorbed ammonia was recorded with a thermal conductivity detector (TCD). In situ pyridine FTIR analysis was performed by flowing pyridine vapor for 30 min to the catalysts, and the excess pyridine was expelled by degassing at 150 °C. Before that, the catalysts were pretreated under vacuum at 500 °C for 1 h, and after that, the temperature was brought down to 150 °C. The structure of catalysts (in the sulfided form) was visualized with the aid of a field emission scanning electron microscope (FESEM) (TESCAN, LYRA 3). Chemical (oxidation) states of the sulfided catalysts elements were evaluated by X-ray photoelectron spectroscopy (XPS) using a PHI 5000 Versa Probe II ULVAC-PHI Inc. spectroscope, and the analysis was conducted with mini Al $K\alpha$ radiation maintained under ultra-high vacuum. During analysis, the chamber's pressure was 9×10^{-8} mBar, while the sample was mounted on the carbon tape. The Avantage software using Gaussian-type baseline was employed for peak deconvolution, and the analysis was corrected for adventitious carbon at 285 eV.

Catalyst sulfidation and activity evaluation

The catalysts (in the pelletized form) were sulfided by first reducing the Co and Mo oxides under the flow of 5% H_2/He at 400 °C for 3 h and presulfiding the reduced metals under the flow of 2 wt.% CS_2 in cyclohexane at 350 °C for 5 h. The HDS activity studies of the activated catalysts were done on a Micro Bench Top Reactor (Parr 4590) ran at a pressure of 5 MPa, temperature of 350 °C and stirring rate of 100 rpm. About 15 ml of fuel in either form of 1000 ppm DBT in dodecane (fuel I) or 1000 ppm MDBT in commercial diesel (fuel II) was added to the reactor vessel containing 25 mg of the activated catalysts. The HDS reaction was run for 3 h after attaining a stabilized reaction condition, and sampling of reaction products was done at one and a half-hour intervals. The amount of sulfur and the reaction products were analyzed using GC-SCD and GC-MS, respectively. The products quantification from the instruments was triplicated to ensure that the uncertainty and errors associated with the instrument are within the acceptable standard, having previously standardized and stabilized the reactor used for the performance of the catalysts.

Results and discussion

Textural properties studies of catalysts

The surface area and pore size distribution (PSD) of all the sulfided catalysts are presented in Table 1. It was observed that the SM and SMC catalysts have nearly the same BET surface area; however, a lower percentage of the BET surface area is available as mesoporous surface area in SMC than in SM. This is ascribed to the loading of Co on the SM catalyst's surface, which blocked some of the mesopores in the support and ultimately led to a decrease in pore size (adsorption branch is used) and pore volume of catalyst and increase in the catalyst microporosity as depicted in Fig. 1. However, incorporating boron to the SM catalyst boosts the BET surface area to 580 m²/g, with almost 90% available as mesoporous surface area. Generally, the introduction of heteroatoms such as Ce and Ti is known to expand the silica structure due to the heteroatoms' relatively large atomic sizes [39, 40]. It was similarly observed that Co to BSM's addition to forming BSMC result in the decrease in BET surface area and porosity of the catalyst, as shown in Fig. 1. The low/small-angle XRD (SAXS) was used to investigate the mesoporosity, pore wall thickness of the pure SBA-15 and the catalysts, and the comparison was made with respect to textural properties at mesoporous level. The pore wall thickness of SBA-15 was found to be 4.68 nm, while the incorporation of Mo and Co without B reduces the thickness. However, upon incorporation of boron in BSM and BSMC, it redisperses the Mo and Co on SBA-15 with better wall thickness closer to reference SBA-15 material synthesized in this study. The SAXS for all the catalysts and SBA-15 is presented as inset in Fig. 1 PSD. The boron effect on the catalyst characteristic outweighs that of cobalt, as evident by surface area, pore volume and pore wall thickness. The elemental analysis of catalyst's components was determined and reported in Table SI-1, the total mole ratio of Co/Co + Mo in BSMC catalyst was found to be 0.29, and a good agreement with the theoretical value at 0.30.

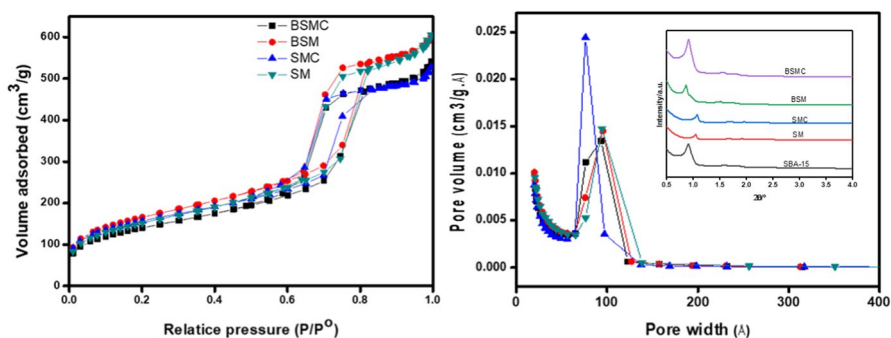


Fig. 1 N₂ adsorption–desorption isotherm of the catalysts and the pore size distribution plot

Diffraction pattern of catalysts

The XRD pattern (Fig. 2 left) of sulfided catalysts shows a broad diffraction peak at nearly $25\ 2\theta$ ($^\circ$) in all the catalysts, and this is ascribed to the amorphous nature of silica-based SBA-15 support [30, 41]. There was no diffraction pattern of boron oxide in all the catalysts, implying the incorporation of boron oxide into the silica framework [42]. Perhaps the amount of boron oxide is below the detectable level by the XRD. Similarly, no diffraction pattern of the active metals oxides was observed except in SM and BSM, where weak peaks at $24, 26$ and $28\ 2\theta$ ($^\circ$) were noticed, and these peaks were assigned to the diffraction pattern of crystalline MoO_3 [43]. This implies that the presence of Co in SMC and BSMC catalysts has enhanced both the dispersion and sulfidation of the MoO_3 in the SBA-15 support, through surface acidity and other characteristics as explained *vide infra*.

Types of acidity by pyridine-FTIR

The presence of Lewis and Brønsted acidity of the catalysts was evaluated by adsorption of pyridine under vacuum using FTIR vibrational spectroscopy. The acidic centers of the catalysts were measured through pyridinium ion peak assignments resulted from acid–base interaction between the pyridine (base) and the acid sites (Lewis and Brønsted). The coordinatively unsaturated ionic metal oxide cations at the surface are related to the Lewis acid sites, while the associated surface OH groups through adsorbed water are assigned to Brønsted sites [44]. As shown in Fig. 2 (right), the strong Lewis site is noticeable at 1450 and $1610\ \text{cm}^{-1}$, while the weak Lewis site peak is extremely low. The contribution from both Lewis and Brønsted acid sites is noticed at $1492\ \text{cm}^{-1}$, with Brønsted acid site peaks observed at 1542 and $1640\ \text{cm}^{-1}$, accordingly. The relative amount of both acidity types gave insights into each catalyst's distribution concerning their composition (see Table 1). The BSM and BSMC possessed higher acidity (Lewis and Brønsted) than SM and SMC, incorporating boron into the catalysts. This observation is expected to bring about an improved performance to both catalysts [45].

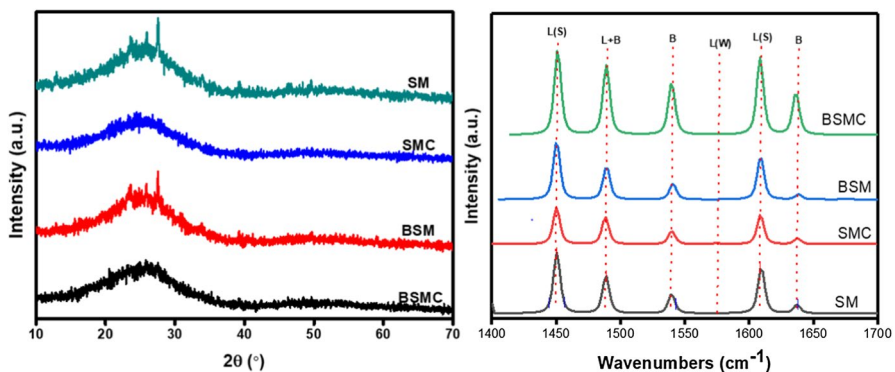


Fig. 2 XRD pattern (left) and pyridine-FTIR (right) of the catalysts

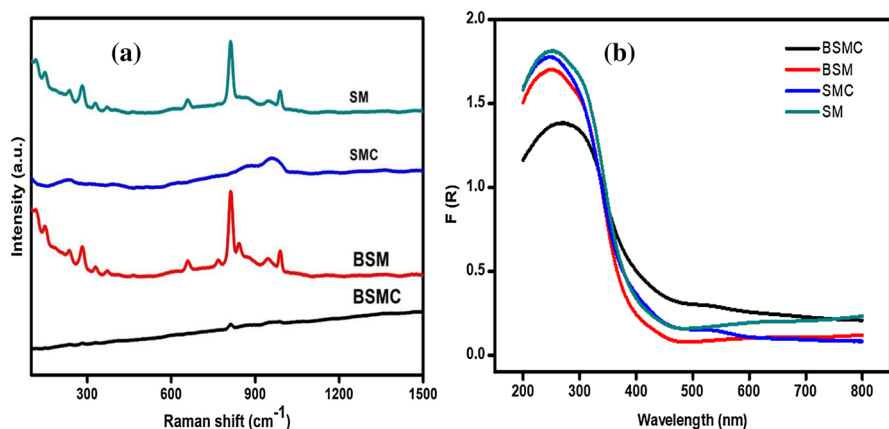


Fig. 3 Raman spectra and DRS-UV-Vis of the catalysts

Table 2 NH₃-TPD and H₂-TPR of the catalysts. (Error = ± 3.0%)

Catalysts	H ₂ -TPR		NH ₃ -TPD	
	Peak Temp. (s)	Quantity (mmol/g STP)	Peak Temp. (s)	Quantity (mmol /g STP)
SM	160, 428, 671	111.1, 13.7, 6.9	239, 654	0.223, 0.007
SMC	133, 429, 670	119.0, 42.1, 12.4	228, 721	0.314, 0.006
BSM	132, 442, 626	122.7, 26.7, 11.0	216, 726	0.317, 0.007
BSMC	137, 438, 620	121.4, 49.0, 14.5	206, 668	0.318, 0.014

H₂-TPR of the catalysts

The H₂-TPR of the catalysts oxides informs the ease of reducing the catalysts, and the amount of H₂ consumed during the reduction process. The catalysts' TPR profiles and the amount of H₂ consumed by the catalysts are presented in Fig. 3 and Table 2, respectively. The main reduction temperatures for MoO₃-MoO₂ and MoO₂-Mo(0) were observed at 428–442 °C and 620–671 °C, respectively. It was noted that the boron-incorporated catalysts present lesser reduction temperature for Mo²⁺-Mo(0) and also have more quantity of consumed H₂ than the corresponding non-boron-containing catalysts. This further confirms that boron aids the dispersion and ease of reducibility of the MoO₃ in the boron-containing catalysts. The ease of reducibility of boron-modified catalysts (BSM and BSMC) pointed to the active phase's availability to a high degree of sulfidation and dispersion, achieved via moderate support interaction for efficient HDS activities.

NH₃-TPD of catalysts

The NH₃-TPD analysis is a useful tool employed to explicate the relative amount of acid sites present in a catalyst oxide [46]. The amount of ammonia desorbed is shown in Table 2, and the TPD profile of the catalysts is shown in Fig. 3b. The TPD profiles showed that desorption occurs in two temperature ranges: 206–239 °C and 654–726 °C, which correspond to weak/moderate acid sites and strong acid sites, respectively [47]. The amount of ammonia desorbed by the catalysts increased in the sequence SM < SMC < BSM ~ BSMC in the 206 – 239 °C temperature range. Precisely, B to SM's addition increases the catalyst's moderate acid sites by 42%, and almost the same acidity effect was noticed upon the incorporation of Co to SM. However, the amount of moderate acid sites in BSMC did not significantly differ from SMC and BSM except in the strong acid sites, which is 100% more than in SMC and BSM. It is largely reported that the number of active sites is related to the amount of surface acidity obtained through the number NH₃ desorbed from the temperature-programmed analysis [7]. Evidently, the boron addition to BSM and BSMC catalysts enhances the surface acidity for efficient HDS reaction.

Raman spectra of catalysts

Raman spectroscopy is a great tool that is often used to understand the Mo compound's chemical structure [48]. The Raman spectra of the sulfided catalysts, presented in Fig. 4a, showed peaks at 605 and 850 cm⁻¹, characteristics of the hydroxyl group's vibrational stretching mode Si–OH and the symmetrical stretching of the Si–O–Si groups due to the SBA-15 support. These peaks are more intense in the SM and BSM catalysts and weaker in the SMC and BSMC catalysts, which implies that the loading of Co has resulted in some Co–O–Si interactions that probably affect the stretching of the Si–OH and Si–O–Si bonding in the SMC and BSMC catalysts. Notably, the Raman peaks characteristics of boron oxide were not observed in both BSM and BSMC catalysts, confirming the XRD results that boron oxide has been incorporated into the SBA-15 framework. Other Raman peaks were observed at 284,

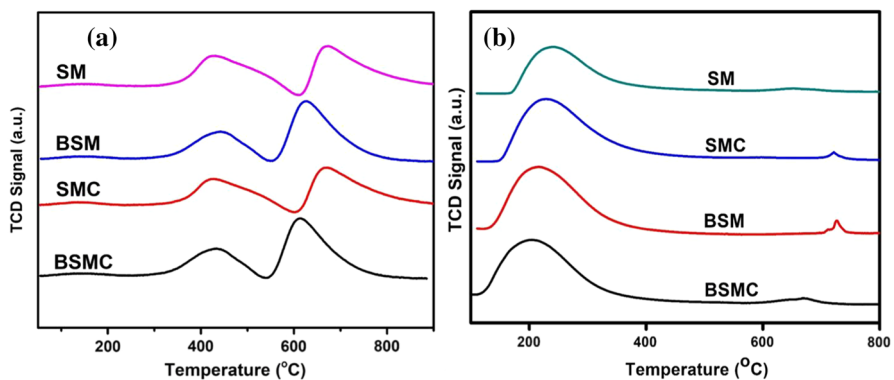


Fig. 4 H₂-TPR and NH₃-TPD of the catalysts in their metal oxide form

650, 810 and 980 cm⁻¹ in SM and BSM catalysts, and these peaks correspond to the wagging, symmetrical and asymmetrical stretching respectively of the Mo–O–Mo in MoO₃. These peaks were mostly in low intensity in the BSMC catalyst, thus affirming that most of the MoO₃ have been reduced and sulfided in the BSMC than in the other catalysts.

UV–Vis (DRS) spectra of catalysts

The DSR is explored to have some insights into the structure and electronic states of catalysts oxides [49]. The DRS spectra of all the catalysts are presented in Fig. 4b, and in all the spectra, there was no absorption band due to SBA-15 since it is transparent in the UV–Vis region of the spectra. The broad absorption band recorded at 200–350 nm in all the catalysts are characteristics of octahedral molybdate, owing to ligand-to-metal charge transfer from oxygen to Mo⁶⁺. It is of particular interest to note that incorporating boron to SM and SMC has led to a significant decline in the absorption band's intensity, which implies that the incorporation of boron has enhanced the metal–support interaction result in better dispersion of the active metals. Furthermore, the presence of single band in BSM and BSMC pointing to the fact that Mo species are mainly ascribed to the polymolybdate O_h Mo types. The absorption band at 520 nm in SMC and BSMC is ascribed to the Co²⁺ in the tetrahedral coordination [49].

FESEM of catalysts

The FESEM analysis of the sulfided catalysts (Fig. SI-1 and Fig. 5) shows dispersed micro-sized hexagonal rods that are consistent with the structure of SBA-15 [50], and the dimension of the rods was noticed to have increased in the boron-modified

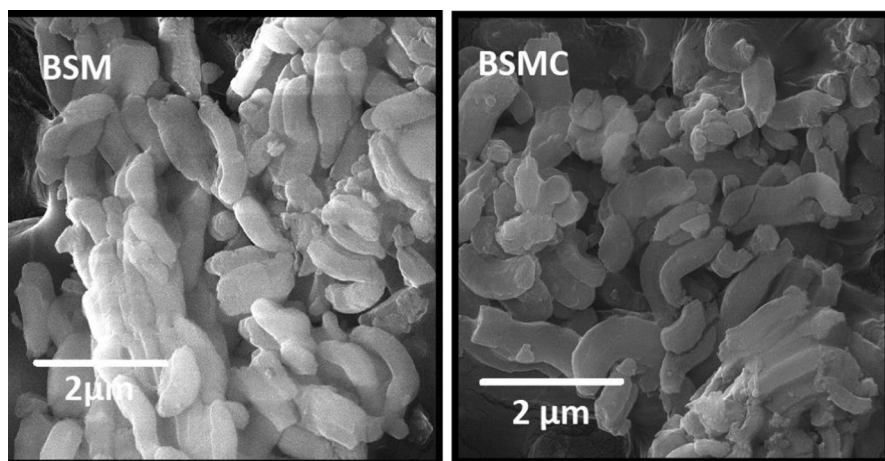


Fig. 5 FESEM of BSM and BSMC catalysts

catalysts, revealing characteristics structure of modified mesoporous SBA-15 [51]. It is essential to mention that the morphology of the SBA-15 was preserved even after incorporating other catalyst's components (Co, Mo, B and S) through their respective precursors. This pointed out that the strategy adopted for preparation is successful, and the ordered mesoporosity properties of the SBA-15 were transferred to the sulfided HDS catalysts. The elemental analysis of sulfided catalysts was observed by EDX as shown in Fig. SI-2-5. It was observed that all catalysts exhibited better dispersion of each component, with emphasis on the boron-incorporated catalyst which showed high dispersion of sulfur.

XPS analysis of the catalysts

The oxidation states of boron, molybdenum and sulfur elements in the catalysts were identified and quantified by analyzing the catalysts XPS spectra. The XPS spectra deconvolution of the catalysts shows that the catalysts (BSM and BSMC) have boron in the chemical state of boric oxide, B_2O_3 (Fig.SI-6) implies that the boron heteroatom is incorporated into the silica structure in the catalysts. The XPS spectra of Mo (Fig. 6) in all the catalysts show that Mo exists in three chemical states:

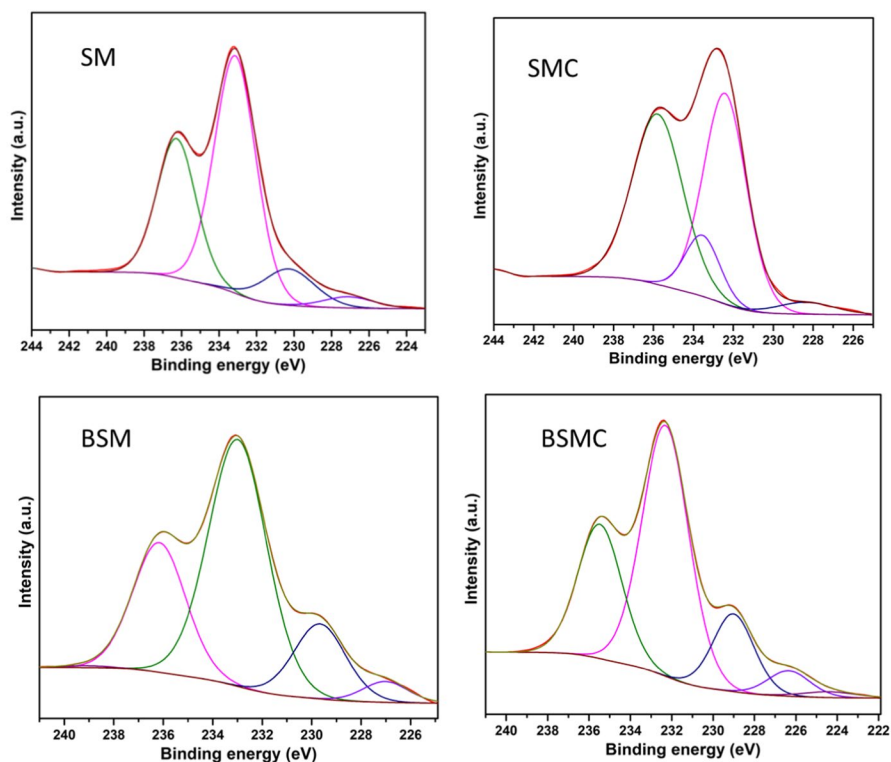
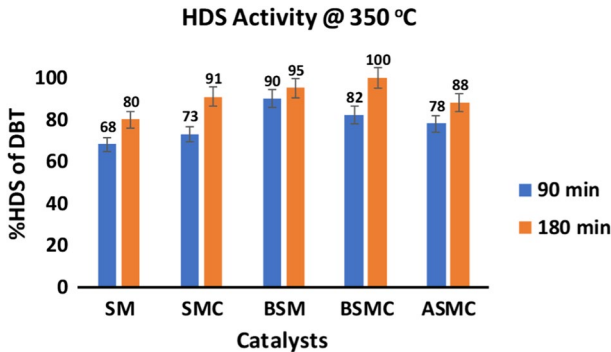


Fig. 6 Deconvoluted XPS spectra of the catalysts showing the chemical states of Mo

Table 3 Atomic percent of chemical states of Mo and S observed in the catalysts

	Mo3d 228.5 eV	Mo3d 231.5 eV	Mo3d 234.8 eV	S2p 162.3 eV	S2p 170.0 eV
SM	–	50.05	23.36	13.93	12.66
SMC	–	48.25	39.41	12.34	–
BSM	9.68	39.95	19.85	19.99	10.53
BSMC	16.02	38.82	18.69	26.47	–

**Fig. 7** HDS performance plot of boron-modified catalysts. Fuel=1000 ppm dibenzothiophene in dodecane

Mo3d_{5/2} (228.5 eV), Mo3d_{5/2} (230.4 eV) and Mo3d_{5/2} (232.5 eV), and these correspond to the (Mo⁴⁺(3d_{5/2})), (Mo⁵⁺(3d_{5/2})) and Mo⁶⁺(3d_{5/2})), respectively [12]. The relative amount (%) of the molybdenum species in all the catalysts is summarized in Table 3. It was observed that BSM and BSMC catalysts have Mo⁴⁺(3d_{5/2}) species, which is an indication of the presence of surface MoS₂ in these catalysts. Also, the percentage of MoS₂ in BSMC was higher than in BSM, which may imply the BSMC catalyst's better reactivity than the others in the series. The sulfur chemical states in the catalysts (Fig. SI-8) also show two sulfur species: the sulfide and the oxysulfide observed at 162.3 eV and 170 eV, respectively. Correspondingly, the sulfide in the catalysts is highest in BSMC, which corroborates the claim that BSMC has more MoS₂ phases than the other catalysts. The incorporation of boron resulted into improved surface acidity, textural properties, better reduction potential and presence of polymolybdate (O_h), which can produce highly reducible and dispersed sulfided phase necessary for efficient HD operation. These observations are supported by TPD, pyridine-FTIR, surface area and porosity, TPR and DRS analysis, respectively.

Catalysts activity studies using fuel I

The catalysts' activity was first studied using fuel I, consisting of 1000 ppm DBT in dodecane. The catalysts' HDS performance plot is presented in Fig. 7, and the summarized percentage conversion is shown in Table SI-2. The percent DBT removal after one and a half hour of HDS reaction for SM catalyst is 68%, and the SMC

has an increased conversion, of 73%, due to the Co-promotion effect. Interestingly, the boron-modified SM catalyst (BSM) showed a much higher conversion of 90%. In comparison, the boron-modified SMC (BSMC) presented conversion of nearly 82% at the one and a half hour of HDS reaction. It was further observed that the percent conversion increases after the three-hour reaction time, and the SMC and BSMC catalysts presented the highest increase, by 19.8% and 17.9% of the initial conversion, respectively, compared to the other catalysts (SM and SMC). The observations show that incorporating boron to SM improved the catalyst activity better than incorporating Co to SM, at least at the initial reaction stage. This is related to both the textural and structural properties of the catalysts. As discussed in Sect. 3.1, the low mesoporous surface area of SMC due to Co incorporation is why the catalyst's HDS activity is lower than that of BSM. More so, the TPR and TPD results have shown that boron heteroatom increased both moderate acid sites and metals dispersion, which are required for better HDS activity. However, the catalysts' activity is subject to its strong resistance to sulfur poisoning due to H₂S gas generation at a longer reaction time. Comparatively, the BSM activity after 3-h reaction time was slightly lower than expected, whereas the BSMC activity is already at 99.9%. The increase in performance of BSMC, which is by almost 18% of the initial conversion, indicated that the HDS reaction is more favored in the presence of both boron and cobalt. It is well reported that the incorporation of promoter (Ni or Co) favors Mo species' dispersion to achieve more Type-II active phase for better conversion of organosulfur compounds [52]. An analogous catalyst containing alumina-modified SBA-15-CoMo (ASMC) was tested and evaluated in the same HDS reaction with DBT to establish the favorable acidity with BSMC. BSMC conversion rates at 90 and 180 min were 4% and 12% higher than the alumina-based catalyst, respectively.

The observed results indicated that the boron being less acidic introduced moderate acidity with excellent active phase dispersion than alumina. The rate constants for the HDS of DBT reaction at both 1.5-h (k_{HDS} (90 min)) and 3-h (k_{HDS} (180 min)) reaction time and their ratio (k_{HDS} (180 min)/ k_{HDS} (90 min)) for all the catalysts (Table SI-2) further support the claim that the BSMC catalyst has higher activity than the other catalysts in the series after 180 min of reaction, and this is due to better structural characteristics such as improved surface area, pore wall thickness, better acidity and presence of highly reducible polymolybdate (O_h) possessed by the catalyst over others. The product analysis of DBT in model fuel was evaluated at a half-hour reaction interval when the HDS catalytic conversion of most catalysts was below 50% except in the BSM catalyst. Generally, the HDS reaction of DBT proceeds via two most noticeable routes; direct sulfur cleavage from organosulfur aromatic ring (known as direct desulfurization, DDS) to form biphenyl (BP). The hydrogenation of the aromatic ring undergoes intermediate products tetrahydrodibenzothiophene (THDBT) and hexahydro-dibenzothiophene (HHDBT) before cleavage of C-S to form cyclohexylbenzene (CHB) as an alternative reaction route [53]. As shown in Table 4, each catalyst's products' distribution varied according to the surface characteristics. BSM and BSMC catalysts' reactivity was higher than SM and SMC at the 30 min reaction interval, as observed by their higher rate constants. This is due to the high amount of Lewis and Brønsted acidity possessed by these catalysts (see Table 1). Furthermore, the predominant reaction route for all catalysts

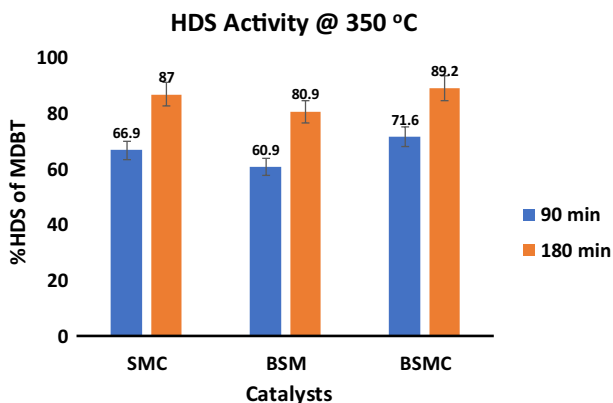
Table 4 Catalyst performance test results: product distribution and first-order rate constants for HDS of DBT at 350 °C at 30 min

Catalysts	%S conversion	Product distribution (wt.%)			$k_{\text{HDS}} \times 10^3$ (min ⁻¹)	$k_{\text{DDS}} \times 10^3$ (min ⁻¹)	$k_{\text{HYD}} \times 10^3$ (min ⁻¹)	$k_{\text{DDS}}/k_{\text{HYD}}$
		CHB	BP	THDBT				
SM	32	16.3	82.6	1.1	12.9	10.6	2.3	4.7
SMC	39	14.8	85.1	0.1	16.5	14.0	2.5	5.7
BSM	52	20.1	76.5	3.4	24.5	18.7	5.8	3.3
BSMC	47	18.6	79.5	1.9	21.2	16.8	4.4	3.9
ASMC	41	22.2	75.4	2.4	17.6	13.3	4.3	3.1

is through direct scission of C–S bond (DDS), while the ratio of reactivity of direct desulfurization to hydrogenation ($k_{\text{DDS}}/k_{\text{HYD}}$) varies. It should be mentioned that the hydrogenation rate constants (k_{HYD}) of BSM and BSMC are higher than SM and SMC, indicating the tendency of the reactant to react through the additional route with sufficient surface acidity as observed by pyridine FTIR [54].

Catalysts activity studies using fuel II

The observed results in Sect. 3.9 motivated the further study of the catalysts' performance in a more complex fuel system that contains 1000 ppm of MDBT dissolved in commercial diesel fuel. The commercial diesel consists of saturated and aromatic hydrocarbons, which can react competitively during the HDS reaction. The refractory sulfur compound, MDBT, can undergo an isomerization reaction before the HDS reaction, and the strength of the catalyst's acid sites significantly affects the isomerization process. The activity of the catalysts in the HDS of MDBT in diesel fuel is plotted in Fig. 8. As expected, the BSMC catalyst performed better than

**Fig. 8** HDS performance plot of boron-modified catalysts. Fuel = 1000 ppm methyl dibenzothiophene in diesel

the other catalysts in the series, and it is observed that the SMC catalyst performs slightly better than the BSM catalyst. This further confirmed the BSM catalyst's high activity is only at ab initio in the dodecane model fuel. In a more complex system like commercial diesel, the activity is low at the onset of the reaction. This low activity is due to the BSM catalyst's moderate acidity and the absence of a Co-promoter. Unlike the BSM, the BSMC has both strong acid sites and Co-promoting effect. There is an electronic interaction due to the B and Co species, typical of a synergetic effect that could withstand the complexity's reaction matrix.

Furthermore, significant surface acidity promotes additional HDS reaction conversion routes through hydrogenation and isomerization, especially for bulky sulfur molecules [55]. The effect of operating temperature on the HDS activity of the BSMC catalyst was further studied using the diesel fuel containing 1000 ppm of MDBT. The observed result (Fig. 9) showed that the catalyst activity increases with temperature. The activation energy (E_a) of the MDBT HDS reaction was subsequently determined using the rate constants obtained at the different temperatures. The E_a was obtained by plotting the natural logarithms of the rate constants versus the reciprocal of the temperatures (in kelvin), and the plot's slope, which is equal to $-E_a/R$, was used to calculate the E_a . The obtained E_a ($77.108 \text{ KJmol}^{-1}$) is lower than most of the previously reported activation energies of MDBT HDS reactions [56–58] which further corroborate the effectiveness of the BSMC catalyst in the HDS reaction of MDBT.

Conclusion

The role of boron heteroatom in the modification of (Co)Mo supported on SBA-15 catalyst has been studied by single-pot preparation of the catalysts. The catalysts: SM, SMC, BSM and BSMC have been tested for the HDS of DBT in dodecane model fuel and HDS of MDBT in commercial diesel. The BSM and BSMC catalysts performed best in the HDS of DBT, whereas the BSMC catalyst possessed superior

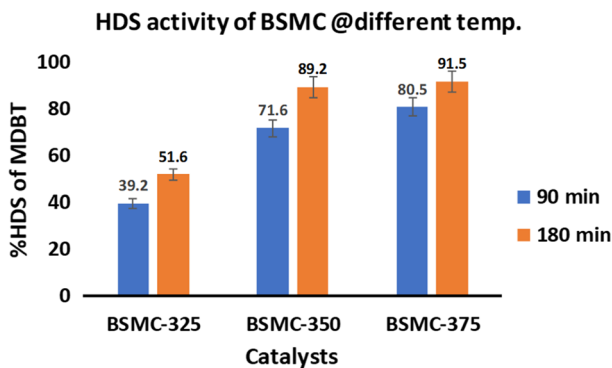


Fig. 9 Effect of process temperature on the HDS performance of BSMC catalyst. Fuel=1000 ppm methylthiobenzothiophene in diesel

activity in the HDS of MDBT. The competitive performance of BSM catalyst in the HDS of DBT relative to SM and SMC catalysts was ascribed to its large mesoporous surface area, moderate acid sites, ease of reducibility and good dispersion of the active Mo metal. The exceptional performance of BSMC in the HDS of both model and diesel fuels is considered due to its strong acid sites, the Co-promoting effect, high degree of sulfidation and dispersion and the electronic interaction between the boron heteroatom and the active metals in the catalyst. The BSMC catalyst is suitable for potential ultradeep HDS of transportation fuels with alkylated derivatives of DBT.

Supplementary Information The online version contains supplementary material available at <https://doi.org/10.1007/s11164-021-04475-x>.

Acknowledgements The financial support provided by King Fahd University of Petroleum & Minerals (KFUPM) for funding this work through Project No. DSR NUS15105 is greatly acknowledged.

References

1. C. Song, *Catal. Today* **77**, 17 (2002)
2. W. Lai, L. Pang, J. Zheng, J. Li, Z. Wu, X. Yi, W. Fang, L. Jia, *Fuel Process. Technol.* **110**, 8 (2013)
3. M. Zhang, J. Fan, K. Chi, A. Duan, Z. Zhao, X. Meng, H. Zhang, *Fuel Process Technol* **156**, 446 (2017)
4. H. Song, F. Zhang, N. Jiang, M. Chen, F. Li, Z. Yan, *Res. Chem. Intermed.* **44**, 5285 (2018)
5. S.T. Hong, D.R. Park, S.J. Yoo, J.D. Kim, H.S. Park, *Res. Chem. Intermed.* **32**, 857 (2006)
6. H. Song, Q. Yu, N. Jiang, Z. Yan, T. Hao, Z. Wang, *Res. Chem. Intermed.* **44**, 3629 (2018)
7. D. Zhang, A. Duan, Z. Zhao, C. Xu, *J. Catal.* **274**, 273 (2010)
8. G. Pérot, *Catal. Today* **86**, 111 (2003)
9. Y. Saih, K. Segawa, *Appl. Catal. A Gen.* **353**, 258 (2009)
10. T. Li, A. Duan, Z. Zhao, B. Liu, G. Jiang, J. Liu, Y. Wei, H. Pan, *Fuel* **117**, 974 (2014)
11. S. Badoga, A.K. Dalai, J. Adjaye, Y. Hu, *Ind. Eng. Chem. Res.* **53**, 2137 (2014)
12. A. Tanimu, S.A. Ganiyu, S. Adamu, K. Alhooshani, *React. Chem. Eng.* **4**, 724 (2019)
13. A.A. Asadi, S.J. Royae, S.M. Alavi, M. Bazmi, *Fuel Process. Technol.* **187**, 36 (2019)
14. A. Safari, M. Vesali-Naseh, *J. Clean. Prod.* **220**, 1255 (2019)
15. Y. Dong, Y. Xu, Y. Zhang, X. Lian, X. Yi, Y. Zhou, W. Fang, *Appl. Catal. A Gen.* **559**, 30 (2018)
16. Q. Gao, Y. Zhang, K. Zhou, H. Wu, J. Guo, L. Zhang, A. Duan, Z. Zhao, F. Zhang, Y. Zhou, *RSC Adv.* **8**, 28879 (2018)
17. X. Zhou, A. Duan, Z. Zhao, Y. Gong, H. Wu, J. Li, Y. Wei, G. Jiang, J. Liu, Y. Zhang, *J. Mater. Chem. A* **2**, 6823 (2014)
18. M.A. López-Mendoza, R. Nava, C. Peza-Ledesma, B. Millán-Malo, R. Huirache-Acuña, P. Skewes, E.M. Rivera-Muñoz, *Catal. Today* **271**, 114 (2016)
19. C. Suresh, L. Pérez-Cabrera, J.N. Díaz de León, T.A. Zepeda, G. Alonso-Núñez, S.F. Moyado, *Catal. Today* **296**, 214 (2017)
20. H. Li, Y. Sakamoto, Z. Liu, T. Ohsuna, O. Terasaki, M. Thommes, S. Che, *Microporous Mesoporous Mater.* **106**, 174 (2007)
21. K. Chandra Mouli, S. Mohanty, Y. Hu, A. Dalai, J. Adjaye, *Catal. Today* **207**, 133 (2013)
22. W. Fu, L. Zhang, T. Tang, Q. Ke, S. Wang, J. Hu, G. Fang, J. Li, F.-S. Xiao, *J. Am. Chem. Soc.* **133**, 15346 (2011)
23. P. Jabbarnezhad, M. Haghghi, P. Taghavinezhad, *Fuel Process. Technol.* **126**, 392 (2014)
24. C.E. Santolalla-Vargas, V.A.S. Toriello, J.A. de los Reyes, D.K. Cromwell, B. Pawelec, J.L.G. Fierro, *Mater. Chem. Phys.* **166**, 105 (2015)
25. J. Chen, F. Maugé, J. El Fallah, L. Oliviero, *J. Catal.* **320**, 170 (2014)
26. R. Palcheva, L. Kaluža, L. Dimitrov, G. Tyuliev, G. Avdeev, K. Jiráťová, A. Spojakina, *Appl. Catal. A Gen.* **520**, 24 (2016)

27. X. Guo, M. Song, X. Zhao, L. Zhao, J. Fuel Chem. Technol. **44**, 1326 (2016)
28. W. Cui, W. Li, R. Gao, H. Ma, D. Li, M. Niu, X. Lei, Energy Fuels **31**, 3768 (2017)
29. O.Y. Gutiérrez, S. Singh, E. Schachtl, J. Kim, E. Kondratieva, J. Hein, J.A. Lercher, ACS Catal. **4**, 1487 (2014)
30. S.A. Ganiyu, K. Alhooshani, Energy Fuels **33**, 3047 (2019)
31. Y. Wang, H. Li, J. Yao, X. Wang, M. Antonietti, Chem. Sci. **2**, 446 (2011)
32. Y. Zheng, Y. Jiao, L. Ge, M. Jaroniec, S.Z. Qiao, Angew. Chemie Int. Ed. **52**, 3110 (2013)
33. A.-M. Alexander, J.S.J. Hargreaves, Chem. Soc. Rev. **39**, 4388 (2010)
34. Y. Cao, H. Yu, J. Tan, F. Peng, H. Wang, J. Li, W. Zheng, N.-B. Wong, Carbon N. Y. **57**, 433 (2013)
35. T.A. Saleh, S.A. AL-Hammadi, A.M. Al-Amer, Process Saf. Environ. Prot. **121**, 165 (2019)
36. A. Usman, T. Kubota, Y. Araki, K. Ishida, Y. Okamoto, J. Catal. **227**, 523 (2004)
37. F. Rashidi, T. Sasaki, A.M. Rashidi, A.N. Kharat, K.J. Jozani, J. Catal. **299**, 321 (2013)
38. D. Zhao, J. Feng, Q. Huo, N. Melosh, G.H. Fredrickson, B.F. Chmelka, G.D. Stucky, Science **279**, 548 (1998)
39. A. Tanimu, K. Alhooshani, Energy Fuels **33**, 2810 (2019)
40. S.A. Ganiyu, S.A. Ali, K. Alhooshani, Ind. Eng. Chem. Res. **56**, 5201 (2017)
41. P. Velmurugan, J. Shim, K.-J. Lee, M. Cho, S.-S. Lim, S.-K. Seo, K.-M. Cho, K.-S. Bang, B.-T. Oh, J. Ind. Eng. Chem. **29**, 298 (2015)
42. Q. Dai, X. Wang, G. Chen, Y. Zheng, G. Lu, Microporous Mesoporous Mater. **100**, 268 (2007)
43. J. Gong, W. Zeng, H. Zhang, Mater. Lett. **154**, 170 (2015)
44. G. Busca, Catal. Today **41**, 191 (1998)
45. S.A. Ganiyu, S.A. Ali, K. Alhooshani, Chem. Sel. **4**, 370 (2019)
46. S.A. Ganiyu, S.A. Ali, K. Alhooshani, RSC Adv. **7**, 21943 (2017)
47. F. Lónyi, J. Valyon, Microporous Mesoporous Mater. **47**, 293 (2001)
48. Y. Li, Z. Feng, Y. Lian, K. Sun, L. Zhang, G. Jia, Q. Yang, C. Li, Microporous Mesoporous Mater. **84**, 41 (2005)
49. J.A. Mendoza-Nieto, O. Vera-Vallejo, L. Escobar-Alarcón, D. Solís-Casados, T. Klimova, Fuel **110**, 268 (2013)
50. S. Che, K. Lund, T. Tatsumi, S. Iijima, S.H. Joo, R. Ryoo, O. Terasaki, Angew. Chemie Int. Ed. **42**, 2182 (2003)
51. S.A. Ganiyu, K. Alhooshani, S.A. Ali, Appl. Catal. B Environ. **203**, 428 (2017)
52. S.L. Amaya, G. Alonso-Núñez, T.A. Zepeda, S. Fuentes, A. Echavarría, Appl. Catal. B Environ. **148**, 221 (2014)
53. S.A. Ali, S. Ahmed, K.W. Ahmed, M.A. Al-Saleh, Fuel Process. Technol. **98**, 39 (2012)
54. Y. Li, K. Chi, H. Zhang, P. Du, D. Hu, C. Xiao, H. Li, Z. Zhao, A. Duan, C. Xu, Fuel Process. Technol. **180**, 56 (2018)
55. Q. Yu, L. Zhang, R. Guo, J. Sun, W. Fu, T. Tang, T. Tang, Fuel Process. Technol. **159**, 76 (2017)
56. J. Ancheyta, M.J. Angeles, M.J. Macías, G. Marroquín, R. Morales, Energy Fuels **16**, 189 (2002)
57. A. Venezia, V. La Parola, G. Deganello, B. Pawelec, J.L. Fierro, J. Catal. **215**, 317 (2003)
58. E. Reséndiz, A. Rosales-Quintero, G. Marroquín, Fuel **86**, 1247 (2007)

Publisher's Note Springer Nature remains neutral with regard to jurisdictional claims in published maps and institutional affiliations.